Suplemento de la Revista Mexicana de Física **5** 011202 (2024) 1–7

Interpretation of X-ray absorption spectra by synchrotron radiation of the uranium mineral species transported by the main stream "El Tigre", in Peña Blanca, Chihuahua, Mexico

C. Hernández-Herrera[a], J. G. Canché-Tello[a], R. M. Cabral-Lares[a,b], Y. Rodríguez-Guerra[a], V. Pérez- Reyes[a], F. G. Faudoa-Gómez[a], H. E. Esparza-Ponce[a], I. A. Reyes-Cortés[c], D. Hernández-Cruz[d], R. Loredo-Portales[e], and M. E. Montero-Cabrera[a]

[a]*Centro de Investigación en Materiales Avanzados, Miguel de Cervantes 120, Complejo Industrial Chihuahua, 31109, Chihuahua, Chih. México.*
[b]*Tecnológico Nacional de México Campus Chihuahua II, Ave. De las Industrias # 11101, Complejo Industrial Chihuahua, 31130, Chihuahua, Chih. México.*
[c]*Facultad de ingeniería, Universidad Autónoma de Chihuahua, Circuito Número I s/n, Nuevo Campus Universitario, Nte. 2, 31125, Chihuahua, Chih. México.*
[d]*Facultad de ingeniería, Universidad Autónoma de Chiapas. Blvd. Belisario Domínguez km 1081 Col. Terán 29050, Tuxtla Gutiérrez, Chis. México.*
[e]*Instituto de Geología, Estación Regional del Noroeste, Universidad Nacional Autónoma de México. Luis Donaldo Colosio s/n, Los Arcos, 83250 Hermosillo, Son. México.*

Received 7 December 2023; accepted 9 January 2024

The state of Chihuahua, Mexico, has several uranium deposits. The most important is the Peña Blanca deposit at north of the Chihuahua City. After an intensive exploration in the 80's, the mineral extracted and unprocessed was confined in rock stacks exposed to weathering. To characterize the transport of uranium by surface water in the form of particles or dissolved, a sampling was carried out in the bed of the stream "El Tigre". Nine sediment samples were collected near the Nopal 1 mine, and separated into coarse sand, fine sand, silt, and fine silt + clay fractions. The activity concentration of the uranium series isotopes was determined by gamma spectrometry, applied to the different fractions of each sample. The fine silt + clay and fine sand fractions were analyzed by X-ray diffraction in the 2 most active samples, Nopal 1 and Nopal 2. The phases are quartz, calcite, montmorillonite, sanidine, orthoclase, albite, kaolinite and magnetite. Particles of $d < 100$ μm (P1-Bulk) were extracted from the fine sand fraction of Nopal 1 with the help of ultraviolet light fluorescence; uranium and silicates were confirmed in them by SEM-EDS. P1-Bulk sample was subjected to X-ray absorption spectroscopy measurements on the U L3-edge, as well as to the samples fine silt + clay fraction of the Nopal 1 (P1-Clay) and Nopal 2 (P1-Silt). The X-ray absorption near edge (XANES) region analyzed indicates the presence of hexavalent uranium in the three samples. The fit of the Extended X-ray absorption fine structure (EXAFS) spectrum of the P1-Bulk sample indicates that it is α-uranophane. This result is consistent with the reports of the area.

Keywords: Uranium; Radiation synchrotron; environmental; Mexico.

DOI: https://doi.org/10.31349/SuplRevMexFis.5.011202

1. Introduction

The Sierra Peña Blanca is located approximately 80 kilometers northeast of Chihuahua City (Fig. 1) [1]; it contains three main uranium deposits: El Nopal, Puerto 3 and Margaritas. The Nopal 1 mine was active between 1969 and 1981, until U mining activity stopped in the region, leaving exposed clusters of material and both surface and subway mines. This deposit consists mainly of minerals such as uranophane, weeksite, carnotite and schoepite, with minor amounts of primary uraninite [2]. It is also located in the Nopal Formation where the upper zone of the formation consists of rhyolitic ash flow tuff, with abundant crystals [3]. The mining district is located in the physiographic province of Basin and Range [4], so its geomorphology corresponds to the characteristics of this, with sierras separated by extensive plains filled with alluvial material from these. Hydrologically, it is located in the region RH34 "Cuencas Cerradas" del Norte [5], which is

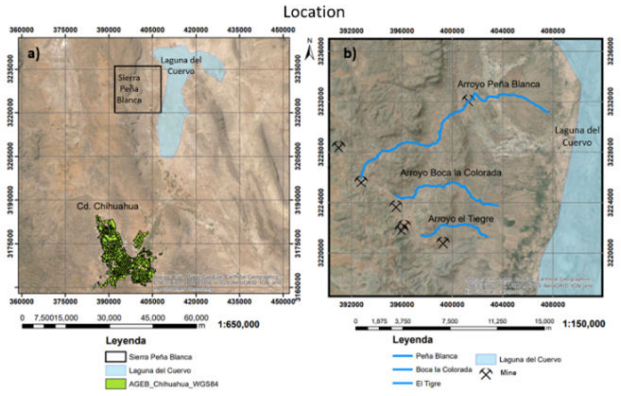

FIGURE 1. a) Location of Sierra Peña Blanca and Laguna del Cuervo with respect to Chihuahua city. b) Location of major streams and mining prospects in the study area.

characterized by torrential rains followed by long periods of drought. Since it is an endorheic basin, the hydrology of the

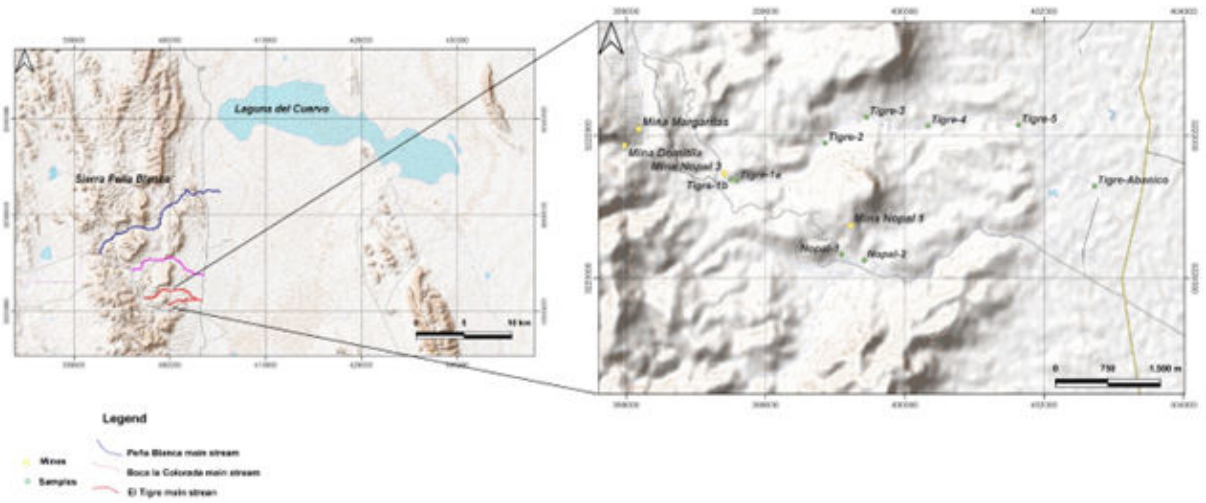

FIGURE 2. Sierra Peña Blanca and Laguna del Cuervo. The location of the sampling points is shown on the right.

area favors the transport of minerals through the main streams in the zone, such as El Tigre stream, which flows into Laguna del Cuervo.

Uranium oxidation states are +3, +4, +5 and +6. In oxidizing environments, uranium is usually found with valence +6 as the highly soluble uranyl ion UO_2 [6]. The dissolution of this element and its presence in the environment depends entirely on the weathering processes of rocks and sediments, as well as its level of exposure to them. The study of environmental radioactivity provides information on the mechanism of uranium transport through surface waters in this particular study.

The isotopes present in nature are ^{234}U, ^{235}U and ^{238}U, the last two being the parents of two radioactive series of successive decays. The ^{238}U presents alpha, beta and gamma successive decays until the isotope ^{206}Pb, which is stable [7]. In geological time, all members of the U decay chain in a deposit are in secular equilibrium, *i.e.*, parent radioisotope activity is equal to that of the daughter radioisotope. This particular study focused on the activities of the members ^{214}Pb, ^{214}Bi and ^{226}Ra.

Due to the health consequences of environmental radioactivity in the Chihuahua's Desert, the sources and their evolution must be characterized from different approaches (chemical, geological, environmental). For this purpose, we will obtain phase analysis of the sediments, morphology and elemental analysis. As well as the radioactivity, the identification of the U oxidation state and the preponderant uraniferous phase in the most active samples of the Tigre stream.

TABLE I. Sampling points.

Sample	Coordinate	
	East	North
Tigre-1a	397590	3221365
Tigre-1b	397498	3221389
Tigre-2	398857	3221895
Tigre-3	399452	3222261
Tigre-4	400334	3222138
Tigre-5	401633	3222151
Tigre-Abanico	402722	3221291
Nopal-1	399098	3220334
Nopal-2	399418	3220253

FIGURE 3. Sampling in El Tigre main stream.

2. Materials and methods

2.1. Sediment sampling

Seven sediment samples were collected along the main stream "El Tigre". The samples Nopal 1 and Nopal 2 were collected from tributaries of streams nearby the Nopal 1 mine (Fig. 2).

It was carried out in the least invasive way possible to the geological environment, following the procedure reported by Colmenero *et al.* [8]. The sample collection area was defined by a square structure with a side of 50 cm (Fig. 3), and each

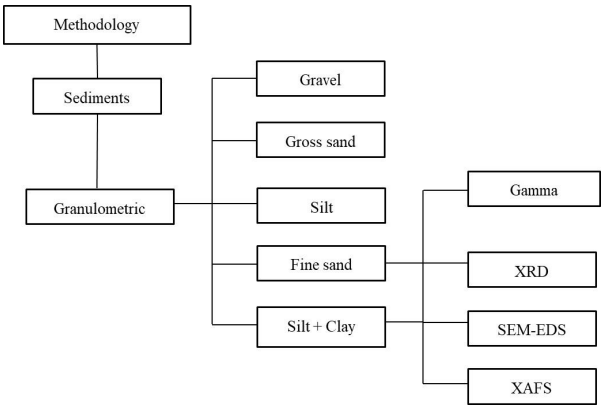

FIGURE 4. Flowchart of the methodology for each sample.

sample was stored in high-density polypropylene bags. Its location coordinates are shown in Table I.

The particle size separation was carried out by vibrating mesh sieving with sizes 16 (1.19 mm), 50 (0.279 mm), 100 (0.149 mm), 200 (0.074 mm) and 400 (0.037 mm), for obtaining coarse sand, fine sand, coarse silt, fine silt and clay particle sizes.

The work plan for the El Tigre mainstream sediment samples is shown in Fig. 4

2.2. Scanning electron microscopy (SEM)

Morphological and composition characterization of the samples were performed using a Jeol JSM 7401F equipment with the microanalysis energy-dispersive spectrograph (EDAX). The acquisition of digital images was performed with secondary (SE) and backscattered (BSE) electrons.

2.3. X-ray diffraction (XRD)

The sediment analysis by XRD was performed using the XPERT-PRO PANalytical equipment. The diffractograms ware collected from 4.9 to 90° in 2θ angle with a step of 0.0130°. CuKα radiation was used (λ=1.5405).

2.4. Gamma spectrometry

The activity concentration of the uranium series isotopes was determined by applying gamma spectrometry to the different fractions of each sample. A hyper pure germanium high resolution gamma spectrometer Canberra model GC2020 with a relative efficiency of 20% was used. The determination of the activities was carried out by the relative method, using as standard the IAEA certified material RGU-1.

The escape of radon gas from the sample container may be a possible cause of the radioactive disequilibrium between ^{226}Ra isotope and its daughters. To avoid this disequilibrium, the vials must be hermetically closed, for around 30 days. The dry sediment samples were deposited in hermetically sealed Teflon vials, to prevent the ^{222}Rn gas escape. After this procedure, the activities of ^{238}U radioactive series

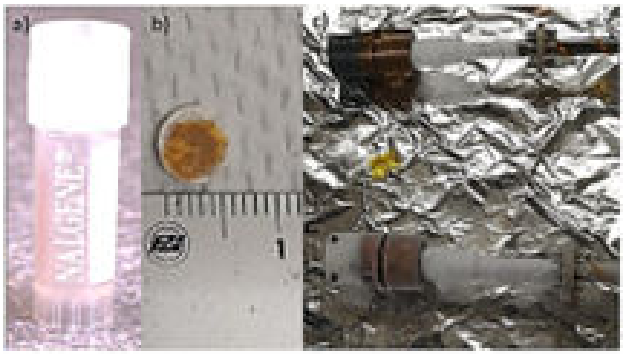

FIGURE 5. a) Vial in beamline I20; b) sample P1 bulk; c) sample holder.

may be obtained considering the ^{234}U in radioactive equilibrium with the ^{226}Ra isotope and its daughters.

For the relative method were used the energy lines from the ^{238}U: ^{234}Th (63.28 keV), ^{226}Ra (186.21 keV) + ^{235}U (185.72 keV), ^{214}Pb (351.93 keV), and ^{214}Bi (609.51 and 1764.49 keV). Then, the activity concentrations of ^{224}Th (equivalent to 238U) and ^{226}Ra by its daughters ^{214}Pb and ^{214}Bi were obtained.

2.5. X-ray absorption spectroscopy

The XAS measurements were performed on the Diamond Light Source (United Kingdom) I20-scanning beamline. For XAS measurements a disc of 6 mm (sample) was enclosed in a sealed plastic vial that was fixed in sample holder and frozen with liquid nitrogen (Fig. 5). X-ray absorption measurements were performed, under normal operating conditions, using a double-crystal Si (111). The measurements were performed in fluorescence mode with individual scans resulting from the average of 11 channels of a Ge fluorescence detector. The energy interval for each point was $\Delta E = 0.3$ eV from the pre-edge zone to the EXAFS region. Then the individual scans were averaged in order to obtain the final experimental spectrum [9]. The normalized absorption signal was obtained through usual data reduction analysis using the program IFEFFIT. The XANES and EXAFS data were processed and analyzed using the suite of programs Demeter (Athena and Artemis) by B. Ravel and M. Newville [10]. The theoretical modeling code FEFF6.0 was used to calculate the backscattering phases and amplitudes of the individual neighboring atoms for the purposes of curve-fitting the data.

3. Results and discussion

3.1. SEM analysis

To identify possible U in the sediments, specific samples of fine silt + clay and particles of fine sand were selected, because they fluoresced under short-wave and long-wave UV light with yellow-green hues (Fig. 6).

Figure 7 shows elemental analysis of a fine sand sedimentary particle (size ~ 0.25 mm) by BSE. The selected

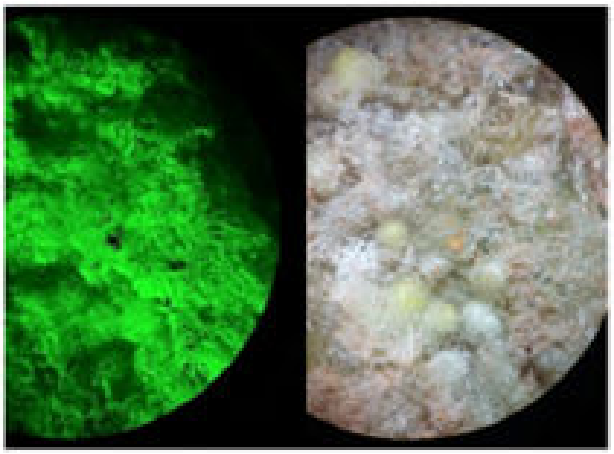

FIGURE 6. Uranium minerals: uranophane and weeksite, covered of chalcedony observed by the stereographic microscope, corresponding to the Nopal mine. In the left image under UV light and in the right image under visible light [11].

area 3 presents 26.48% of uranium in weight. This particle represents a hard agglomerate of different compositions as observed.

3.2. XRD analysis

Figure 8 shows the experimental diffraction patterns of fine sand and fine silt + clay samples, extracted close to Nopal 1 mine. The patterns are similar; eight crystalline phases were identified: quartz, calcite, feldspar (orthoclase, sanidine, albite), montmorillonite, kaolin and magnetite. These results are consistent with previous report by Faudoa F. [11].

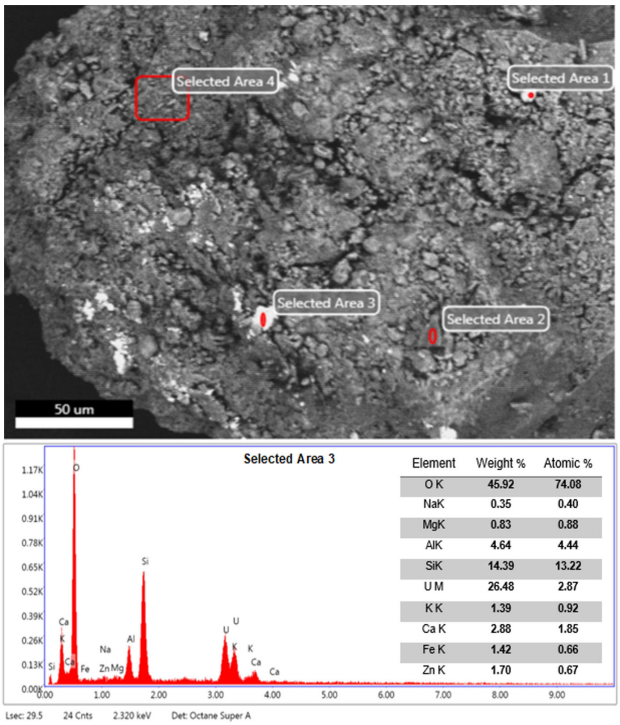

FIGURE 7. Top: Backscattered electron image of Nopal 1 sediment in fine sand. Bottom: Elemental analysis by EDS.

3.3. Gamma spectrometry analysis

Table II displays the activity concentrations and uncertainties for the sedimentary samples of fine sand, and silt-clay. The activities and their uncertainties were obtained according to

TABLE II. Activity concentration in Bq/kg for sediment samples by gamma spectrometry.

Sample	Granulometry	Isotopes		
		Pb-214	Ra-226	Bi-214
Tigre-1a	Fine silt+clay	120±2	102±7	123±3
	Fine sand	123±2	109±5	123±2
Tigre-1b	Fine silt+clay	133±2	103±7	131±3
	Fine sand	142±2	118±5	145±2
Tigre-2	Fine silt+clay	98±2	75±7	101±3
	Fine sand	79±1	L.D.	90±2
Tigre-3	Fine silt+clay	96±2	65±6	91±3
	Fine sand	85±2	65±5	89±2
Tigre-4	Fine silt+clay	76±2	61±6	72±2
	Fine sand	77±1	54±4	79±2
Tigre-5	Fine silt+clay	82±2	73±7	82±3
	Fine sand	71±1	52±4	73±2
Tigre-Abanico	Fine silt+clay	83±2	59±6	85±3
	Fine sand	73±2	55±4	78±2
Nopal-1	Fine sand	95±2	98±5	100±2
Nopa2-1	Fine sand	217±2	214±6	223±9

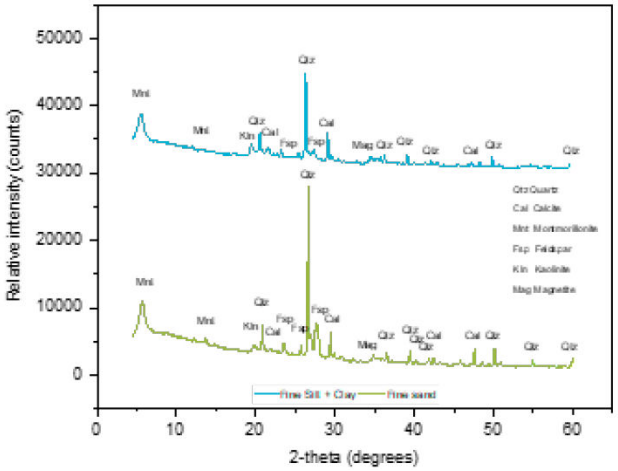

FIGURE 8. Diffraction patterns of sediment samples from Nopal 1, fine sand (green) and fine silt + clay (blue).

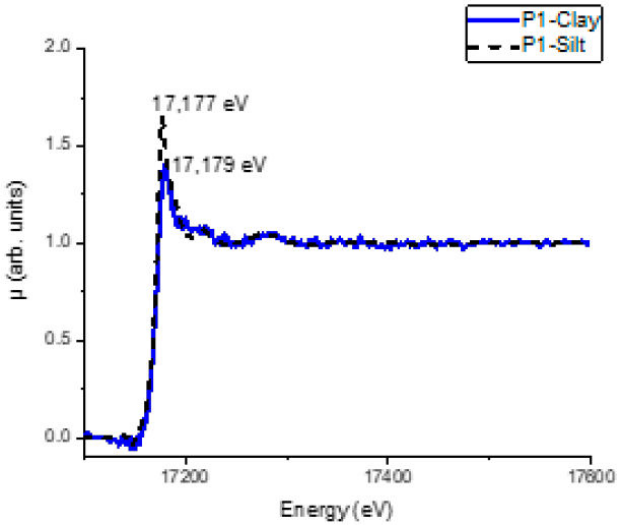

FIGURE 9. Absorption spectra for the P1-Clay and P1-Silt visualized in Athena.

Gilmore's recommendations [12]. The activity of ^{234}U (which also cannot be calculated directly in gamma spectrometry) can be assumed equal to the activity of its radioisotope daughter, ^{226}Ra, if the environment is oxidizing. The ^{226}Ra activity was calculated according to the Gilmore method [12] through the intensity of the 186 keV doublet.

It may be observed that the samples taken in points from Nopal 2 and Tigre 1b present the greatest activities. They were collected near the Nopal I and Nopal III mines, respectively. The activity concentrations in the samples of fine sand, closer to the "Peña Blanca" mountain are higher than the clays. According to the results presented, the fine sands could contain mineral uranium in fragments.

3.4. X-ray absorption spectroscopy analysis

XAS was applied at the U L_3 - edge to the most radioactive samples to identify the uranium phases. The silt + clay fraction 17177 eV (P1 - Silt) and 17179 eV (P1 - Clay). Above 17200 eV start the EXAFS oscillations associated with the photoelectron scattering from the closest oxygen atoms to the absorbing U.

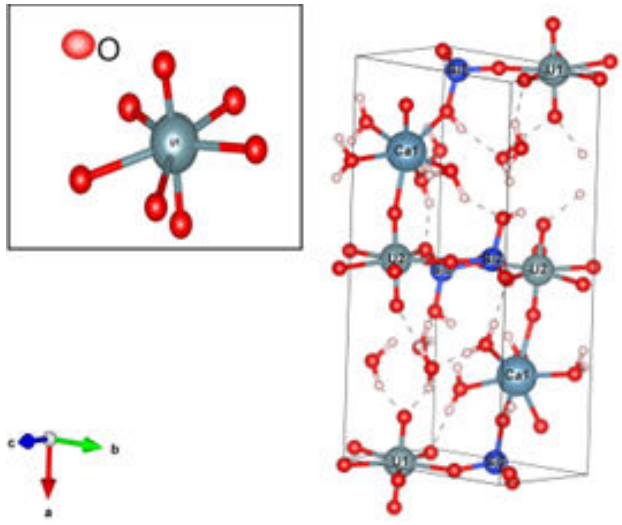

FIGURE 10. The Fourier Transforms (R space) and the k3-weighted (k space) of experimental (solid) and fitted (dashed line) U LIII EXAFS.

TABLE III. EXAFS parameter for P1-Bulk.

Name	Path	N	$S_0{}^2$	σ^2	E_0	ΔR	Reff	Reff+ΔR	Uncert.
Oax	O3.1	2	1.05	0.0063(6)	9	0.009	1.8045	1.814	0.004
Oeq1	O9.1	1	1.05	0.0035(9)	9	-0.039	2.2411	2.202	0.007
Oeq1	O7.1	2	1.05	0.0035(9)	9	-0.039	2.2952	2.256	0.007
Oeq2	O7.2	2	1.05	0.014(5)	9	-0.038	2.4498	2.412	0.019
triangle	O1.1_O9.1	6	1.05	0.010(1)	9	0.010	3.4707	3.481	0.001
Rattle	O3.1_O3.1	2	1.05	0.013(1)	9	0.018	3.6089	3.627	0.008
Si	Si1.1	1	1.05	0.010(4)	9	0.003	3.1444	3.145	0.031
Forward through absorber	O3.1_U_O3.1	2	1.05	0.013 (1)	9	0.018	3.6089	3.627	0.008
U	U1.1	2	1.05	0.02(1)	9	-0.164	3.9241	3.760	0.059

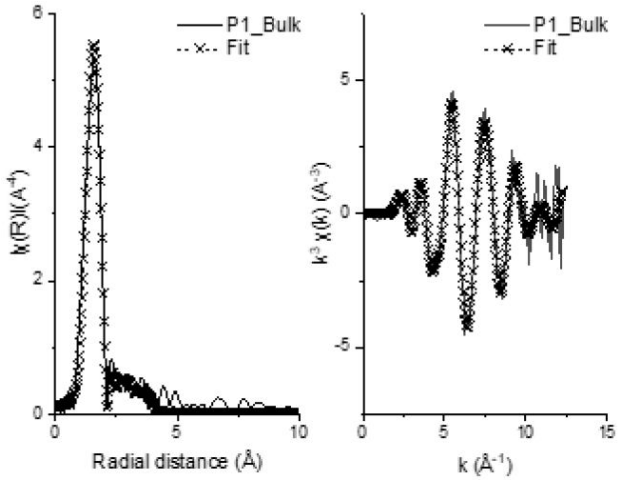

FIGURE 11. The Fourier Transforms (R space) and the k3-weighted (k space) of experimental (solid) and fitted (dashed line) U L_{III} EXAFS.

The inflection point E_0 has been found at 17172.5 eV (P1 -Clay), which is similar to E_0= 17172.3 eV, reported by Bes *et al*., [13] for U^{6+} valence state. The uncertainty of this determination is of order of the step $\Delta E = 0.3$ eV, mentioned above. For fitting the experimental spectrum for P1-Bulk the structural modeling for the fit α-uranophane (Ginderow) [14] is shown in Fig. 10. The Fourier transforms and the k^3-weighted of the EXAFS spectra and fits for the P1-Bulk sample can be seen in Fig. 11. The peaks around 1.3 - 2.5Å arise from the backscattering caused by oxygen atoms nearest to the uranium. A peak at 3.1Å is attributable to the backscattering from the nearest Si neighbor. The best fit to the data parameters are shown in Table III. These results are consistent with a previous report by Kelly [15]. The results of the fit suggest that the model is correct, and therefore, that the oxidation state in U^{6+} and that the radioactivity of these sediments is probably due to the presence of α-uranophane particles.

4. Conclusions

The uranium radioactivity concentration is higher in the sampling points closest to the Nopal I and Nopal III mines. Gamma spectrometry has shown that the location of samples in relation to uranium sources (mines) influences the isotope concentration.

The EXAFS spectrum in P1-Bulk suggests that the uraniferous material present in the sample point Nopal 1 is uranophane. It was also found that the uranium present in the samples silt - clay samples close to Nopal I mine is oxidized (with valence +6).

Acknowledgments

The work described here was funded by CONAHCYT research project CF-2019/10853. XAFS measurements were performed as part of the proposal SP31873 at Diamond Light Source (UK).

1. S. Angiboust *et al*., Structural and biological control of the Cenozoic epithermal uranium concentrations from the Sierra Peña Blanca, Mexico., *Miner. Deposita* **47** (2012) 859, https://doi.org/10.1007/s00126-012-0408-5.
2. P. F. Dobson *et al*., Stratigraphy of the PB-1 Well, Nopal I Uranium Deposit, Sierra Peña Blanca, Chihuahua, Mexico., *Int. Geol. Rev.* **50** (2010) 959, https://doi.org/10.2747/0020-6814.50.11.959.
3. D. Cárdenas-Flores, Uranium deposits in volcanic rocks, Chihuahua, Mexico., Committee Meeting on Uranium Deposits in Volcanic Rocks, Organized by the International Atomic Energy Agency (1985)
4. INEGI., Provincias y subprovincias fisiográficas(Mapa digital), 1:1 000 000. INEGI (2001)
5. CONAGUA., Actualización de la disponibilidad media anual de agua en el acuífero Laguna de Hormigas (0824), estado de chihuahua. CONAGUA (2020)
6. F. Chabaux *et al*., Chapter 3 U-Series Geochemistry in-Weathering Profiles, RiverWaters and Lakes., *Radioact. Environ.* **13** (2008) 49, https://doi.org/10.1016/S1569-4860(07)00003-4.
7. Y. H. Dawood, Factors controlling uranium and thorium isotopic composition of the streambed sediments of the River Nile, Egypt., *JAKU: Earth Sci.* **21** (2012) 77, https://doi.org/10.4197/ear.21-2.4.
8. L. C. Sujo *et al*., Uranium-238 and thorium-232 series concentrations in soil, radon-222 indoor and drinking water concentrations and dose assessment in the city of Aldama, Chihuahua, Mexico., *J. Environ. Radioact.* **77** (2004) 205, https://doi.org/10.1016/j.jenvrad.2004.03.008.
9. L. T. Townsend *et al*., Neptunium and Uranium Interactions with Environmentally and Industrially Relevant Iron Minerals., *Minerals* **12** (2020) 165, https://doi.org/10.3390/min12020165.
10. B. Ravel and M. Newville, ATHENA, ARTEMIS, HEPHAESTUS: data analysis for X-ray absorption spectroscopy using IFEFFIT., *J. Synchrotron Rad.* **12** (2005) 537, https://doi.org/10.1107/S0909049505012719.
11. F. G. Faudoa, Modelo de la evolución de las especies minerales superficiales de uranio de la Sierra Peña Blanca, Chihuahua, México, Centro de investigación en materiales avanzados (CIMAV). (2023).
12. G. Gilmore, Practical Gamma-ray Spectrometry, 2nd ed. (John Wiley & Sons, Ltd, Warrington, UK, 2008), pp. 319-322.
13. R. Bes *et al*., Use of HERFD-XANES at the U L3- and M4-Edges To determine the uranium valence state on $[Ni(H_2O)_4]_3[U(OH,H_2O)(UO_2)8O_{12}(OH)_3]$, Inorg. Chem.

55 (2016) 4260, https://doi.org/10.1021/acs.inorgchem.6b00014.

14. D. Ginderow, Structure de l'uranophane alpha, $Ca(UO_2)_2(SiO_3OH)_{2.5}H_2O$., Acta Cryst. **44** (1988) 421, https://doi.org/10.1107/S0108270187011491.

15. S. D. Kelly, Chapter 14-Uranium Chemistry in Soils and Sediments., *Dev. Soil Sci.*, **34** (2010) 411, https://doi.org/10.1016/S0166-2481(10)34014-1.